Journal of
Applied Remote Sensing

Multispectral imaging systems on tethered balloons for optical remote sensing education and research

Joseph A. Shaw
Paul W. Nugent
Nathan A. Kaufman
Nathan J. Pust
Devin Mikes
Cassie Knierim
Nathan Faulconer
Randal M. Larimer
Angela C. DesJardins
W. Berk Knighton

Multispectral imaging systems on tethered balloons for optical remote sensing education and research

Joseph A. Shaw,[a] Paul W. Nugent,[a] Nathan A. Kaufman,[a] Nathan J. Pust,[a] Devin Mikes,[a] Cassie Knierim,[b] Nathan Faulconer,[a] Randal M. Larimer,[a,c] Angela C. DesJardins,[c] and W. Berk Knighton[c,d]

[a]Montana State University, Electrical & Computer Engineering Department, Bozeman, Montana 59717
jshaw@ece.montana.edu
[b]Montana State University, Physics Department, Bozeman, Montana 59717
[c]Montana State University, Montana Space Grant Consortium, Bozeman, Montana 59717
[d]Montana State University, Chemistry and Biochemistry Department, Bozeman, Montana 59717

Abstract. A set of low-cost, compact multispectral imaging systems have been developed for deployment on tethered balloons for education and outreach based on basic principles of optical remote sensing. They have proven to be sufficiently capable, and they are now being used in research as well. The imagers use tiny complementary metal-oxide semiconductor cameras with low-cost optical filters to obtain images in red and near-infrared bands, and a more recent version includes a blue band. The red and near-infrared bands are used primarily for identifying and monitoring vegetation through the normalized difference vegetation index (NDVI), while the blue band can be used for studying water turbidity and so forth. The imagers are designed to be carried by tethered balloons to altitudes currently up to approximately 50 m. These undergraduate-student-built imaging systems are being used by university and college students for a broad range of applications in multispectral imaging, remote sensing, and environmental science. [DOI: 10.1117/1.JRS.6.063613]

Keywords: multispectral imaging; remote sensing; optical system design; optics education.

Paper 12350P received Oct. 5, 2012; accepted for publication Nov. 10, 2012; published online Dec. 10, 2012.

1 Introduction

Helium-filled balloons or kites have been used to carry lightweight, often low-cost, remote sensing imaging systems for a plethora of applications, including mapping vegetation for agriculture when satellite resolution is too coarse,[1] obtaining large image sets for use in developing remote sensing algorithms,[2] monitoring large-area disaster sites,[3] mapping glacial morphology,[4] and mapping historical archeological sites where aircraft over-flights often are not allowed.[5–7] These types of imagers fill a low-altitude niche to supplement the capabilities of other airborne remote sensing systems, such as uninhabited aerial vehicle (UAV)-borne[8,9] and space-borne imagers for agricultural sensing.[10,11]

Spectral imaging from tethered balloons also provides a wide array of opportunities for students to gain experience with and learn about light, the interaction of light with natural objects, and the use of digital imaging systems in remote sensing for studying the natural environment. We adopted this as a theme for a NASA minority-serving-institution partnership project involving Montana State University (MSU) in Bozeman, Montana, and seven Native American tribal colleges in Montana (Blackfeet Community College, Salish Kootenai College, Aaniiih Nakoda College, Stone Child College, Fort Peck Community College, Little Big Horn College, and Chief Dull Knife College). The goals of the project were for a team of undergraduate students at MSU-Bozeman to design and build eight copies of a two-channel spectral imager and deliver them with documentation to the Tribal Colleges, where students would use them in environmental

0091-3286/2012/$25.00 © 2012 SPIE

science projects with financial support from NASA through the Montana Space Grant Consortium.

The imaging systems were to be built with a parts cost no greater than $1000 and provide simultaneous images in the red and near-infrared (NIR) portions of the spectrum from a tethered balloon that rises to an altitude of approximately 50 m (above which Federal Aviation Administration clearance is required). The requirement for simultaneous images is driven by the instability of the balloon platform, which would make it very difficult to align time-sequential images in different spectral bands. It was required that operators on the ground have the ability to view images in real time and to trigger image acquisition when the desired scene was in the imager's field of view. The balloon payload was limited to 2.3 kg, and it was desired to operate each imager for 1 h or longer without charging batteries. Finally, a ground-based calibration target was required for each imager, thereby enabling real-time calibration of the images to determine the reflectance at each pixel.

2 Imaging System Design

The low-cost, balloon-based imaging systems designed in this project were inspired by our use of multispectral imaging of vegetation for detecting CO_2 gas leaks through the resulting reflectance changes.[12–14] Hyperspectral imaging also has been employed for similar purposes.[15–17] This research was conducted at an agricultural field west of the MSU-Bozeman campus, with support through the Zero Emissions Research and Technology (ZERT) center at Montana State University.[18] In multispectral imaging experiments at the ZERT site, red and NIR images of the vegetation reflectance are acquired, from which a gas leak location is identified through statistical analysis of the reflectances and the normalized difference vegetation index (NDVI), calculated as

$$\mathrm{NDVI} = \frac{\rho_n - \rho_r}{\rho_n + \rho_r}. \tag{1}$$

In this equation, ρ represents the reflectance for red and near-infrared bands, corresponding to approximately 630 to 680 nm and 770 to 820 nm, respectively, for the system the balloon imagers are designed to loosely mimic.[13] Because of chlorophyll absorption, healthy vegetation absorbs in the red and reflects strongly in the NIR, beyond the so-called "red edge" at 700 nm.[18] Reflectance spectra measured with a hand-held spectrometer at the ZERT site for healthy and stressed vegetation are illustrated in Fig. 1, showing that for stressed vegetation the red reflectance rises while the NIR reflectance falls. Therefore, a high NDVI value indicates

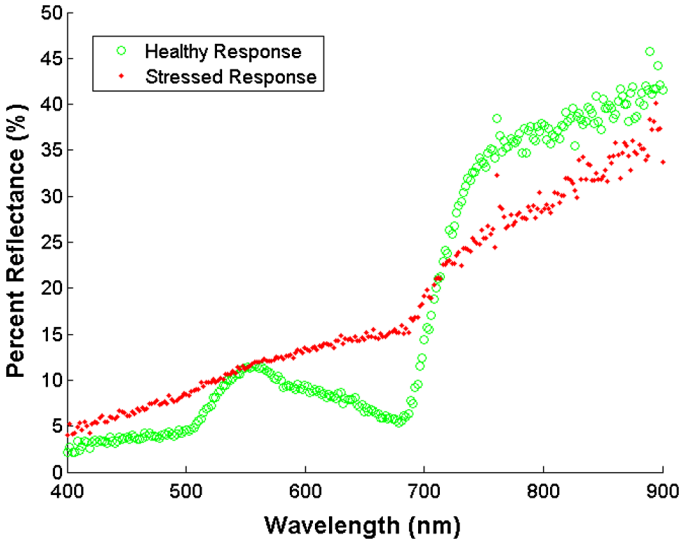

Fig. 1 Visible and NIR reflectance spectra measured for healthy (green circles) and stressed vegetation (red dots).

healthy vegetation, and because of a much flatter red-NIR transition, smaller or even negative NDVI values can indicate the presence of a material ranging from stressed vegetation to urban materials.

Our balloon-borne imagers were designed to allow students to explore the use of the NDVI and related reflectance-based remote sensing in the red and near-infrared spectral region. The response of the imagers can be moved to other spectral bands by replacing the optical filters that are situated directly in front of the ultra-low-cost complementary metal-oxide semiconductor (CMOS) cameras. For simplicity, and because we only needed two spectral channels (later three), we chose to use multiple cameras, each viewing through its own spectral filter. Certainly more sophisticated (and generally more costly) approaches could be adopted, including a pixelated array of color filters on a detector array,[19] multiple detector arrays behind dichroic beam splitters,[12] or an array of tiny lenses with individual spectral filters in front of a single detector array.[20] Rotating filter wheels can be used on stationary platforms[13] but not practically on balloons. Many more variations exist for multispectral imager designs, including division-of-time, division-of-aperture, division-of-wavefront, and division-of-focal-plane designs that are common in spectral and polarization imaging.[21] Our choice to use multiple cameras was driven by the ultralow camera cost and overall optical simplicity, but made necessary the development of post-processing software used to manually align image pairs.

Figure 2 is a photograph of one of the imaging systems that was built at MSU-Bozeman for use at a tribal college. The two circular objects near the left of this picture are optical filters that define the two spectral bands. These filters are optically sealed to the front of the lenses of two tiny CMOS cameras. Just to the right of the cameras and filters is a nickel-metal-hydride (NiMH) 12-v battery, and to the right of that are the electronics boards. The two boards at the top right of the picture are used to record images from each camera onto two secure digital (SD) cards, and the bottom-right board contains a consumer-grade webcam removed from its housing. This webcam provides a live view that is transmitted to the ground via a 2.4-GHz Wi-Fi link that uses the black antenna in this picture. The white antenna on the front side is for a 2.4-GHz ZigBee link that allows the ground-based operator to trigger image acquisition through a dual-channel, ZigBee-controlled relay.

In a second phase of the project, we designed and built an enhanced version of the balloon-borne multispectral imager with a blue-green channel along with the original red and NIR ones (Fig. 3). This second-generation system also had a significantly improved live balloon-to-ground video link and an even lower weight (1.0 kg, compared to 1.45 kg for the two-channel imager) and longer battery life (~3 h, up from ~2). The new system uses a 5.8-GHz video transmitter to send the live video from one of the three CMOS cameras. A three-way switch on the imager module is used while the imager is on the ground to select which camera's output is viewed on

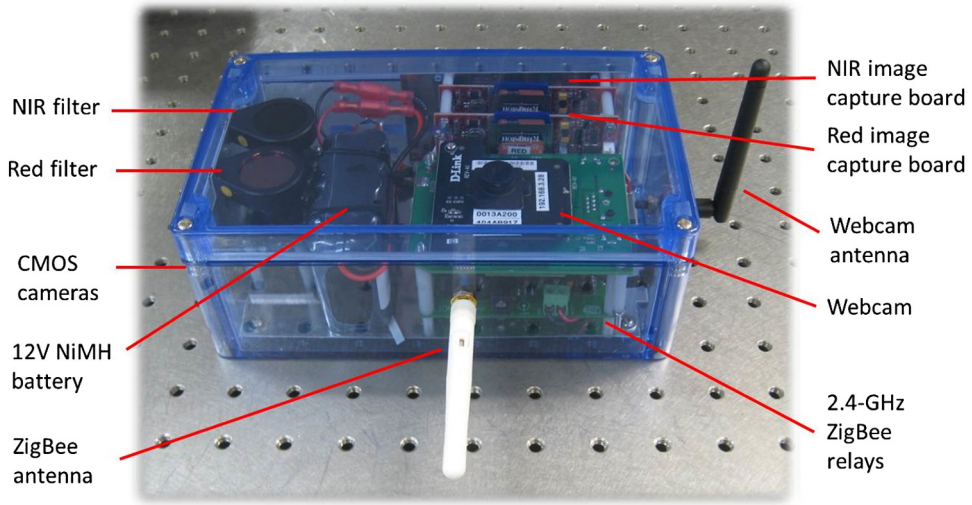

Fig. 2 Photograph of original two-channel, balloon-borne, multispectral imager with primary subsystems labeled.

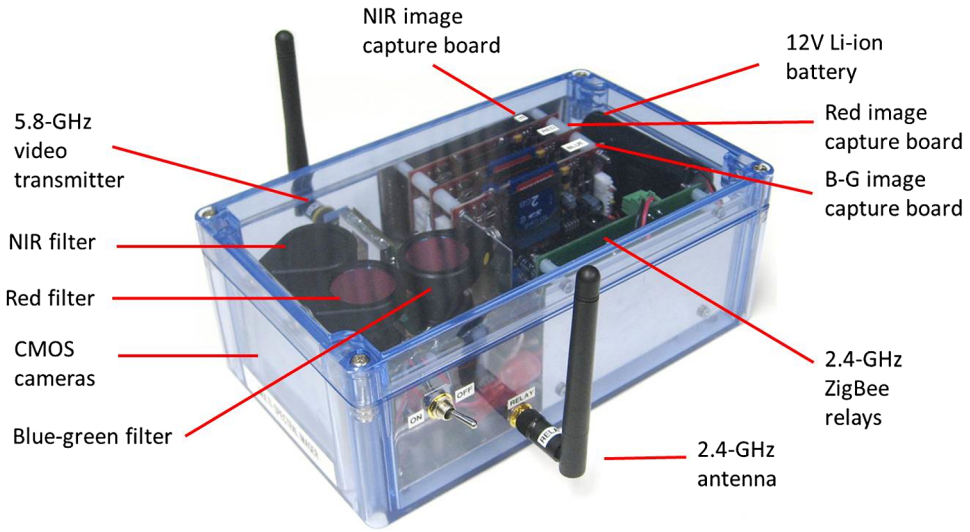

Fig. 3 Photograph of second-generation, three-channel imager with primary subsystems labeled. This version has three spectral channels: blue-green, red, and NIR.

the live video feed. An operator then uses a laptop computer with a ZigBee transmitter and custom software to trigger an image acquisition when the camera's field of view contains the desired object.

Because the tethered balloon is flown at a relatively low altitude (~50 m), we chose cameras and lenses with a wide-angle field of view. The chosen camera was from Electronics123 (model M3186A, cost = 27.50 US) with a full-angle field of view approximately equal to 65×50 deg with 510×492 pixels. Therefore with the balloon at 50 m altitude, the imager could see an area on the ground with approximate dimensions of 64×46 m, with approximately 12-cm pixel resolution.

Although the wide-angle field of view is convenient for imaging relatively large areas, such large incident angles cause the spectral response of interference filters to shift toward shorter wavelengths with a distorted filter response curve. Therefore interference filters must be avoided whenever possible. This also is in accordance with the need to minimize cost, as interference filters can be fairly costly. Our solution was to use gel filters wherever possible. Gelatin filters can be purchased at low cost at photographic supply stores and have quite wide spectral response with effectively zero angle dependence. We used a commonly available visible-block, NIR-pass, filter to define the short-wave cutoff of the NIR channel, as shown in Fig. 4(a). The long-wave cutoff for this filter (not shown in the figure) is established at approximately 1000 nm by the CMOS camera response, which typically decays rapidly beyond about 900 nm for silicon detectors.[22] The red channel was more problematic, as the standard red gel filter transmits both

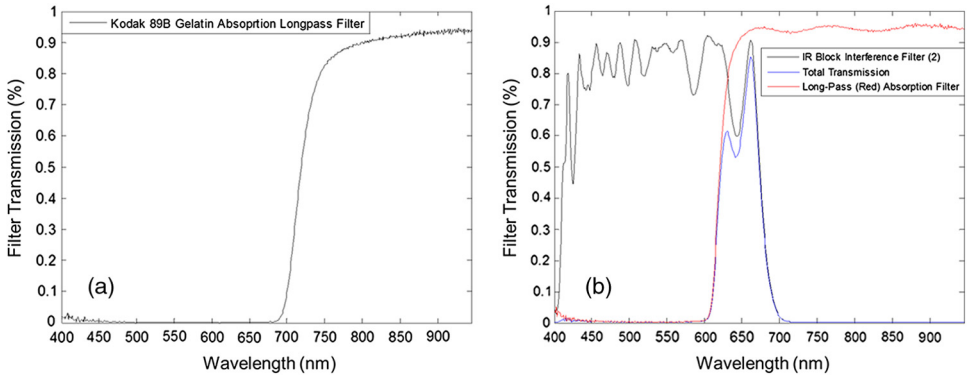

Fig. 4 Spectral transmission functions for the (a) NIR filter and (b) red filter, comprising an IR-block filter (left curve shown in black) stacked with an IR-pass filter (right curve shown in red). The center curve shown in blue is the net on-axis red transmittance.

red and NIR. Therefore we stacked the red gel filter with two NIR-blocking interference filters that pass wavelengths shorter than 700 nm. The product of these transmission curves produces a red bandpass filter with half-power transmission wavelengths of approximately 620 and 670 nm, as shown with the center blue line in Fig. 4(b).

As a result of the use of an interference filter to remove the NIR portion of the red gel filter transmittance, pixels at the edge of the field of view experienced a red-channel transmittance that was lower in amplitude and shifted to shorter wavelengths. We accounted for this by measuring the net filter transmittance spectrum using a spectrometer, while the filter was rotated to different angles in front of a uniformly illuminated integrating sphere. The measured response is shown in Fig. 5 for incidence angles of 20 deg (a) and 40 deg (b). It is apparent from these plots that the angle-dependent response must be accounted for, and in our system this is done in post-processing on the ground, using custom image-processing software.

Figure 6 illustrates an important point that must be considered when using any filters, but especially low-cost gel filters. Here, as is quite common, the blue-green gel filter has a well-defined blue-green band with half-power wavelengths near 440 and 540 nm, but it has even higher transmittance at NIR wavelengths beyond 700 nm. This "out-of-band" transmittance was removed by combining the blue-green gel filter with two more of the NIR-blocking filters used in the red channel, resulting in the blue-green channel response shown in Fig. 6 with zero NIR response.

An additional optical characterization had to be implemented for the enclosure transmittance. The imaging system enclosures isolate the optics and electronics from the weather but have a significantly lower transmittance in the blue relative to the other channels. Therefore, in the second-generation systems, the post-processing software includes a step to divide out the measured enclosure transmittance to maintain blue-channel calibration. The enclosure's transmittance was found to be relatively flat in all channels other than blue-green. Fortunately, there was no angle dependence of the enclosure transmittance.

The low-cost CMOS cameras use automatic gain control to continually adjust for the varying scene brightness levels. Because there is no way to control this feature on these cameras, it was necessary to use a ground-based calibration target to turn the recorded image digital numbers into reflectance values. An early example was constructed by painting the two halves of a plywood sheet black and white (Fig. 7). Later calibration targets were painted canvas tarps, which allowed much easier transport to a field site. The reflectance spectrum was measured for the black and white portions using a hand-held spectrometer and a Spectralon 99%-reflective calibration reference target. The image-processing software incorporates these measured spectra and uses them, along with the measured filter response curves, to calculate the reflectance for each pixel of each image. However, because of the large amount of angular response falloff inherent in these low-cost cameras, this approach also required that we use a uniform integrating-sphere source to create a map of camera response versus pixel number. This map also is incorporated in the image-processing software to relate the other image pixels to the pixels containing the black-and-white calibration reference regions.

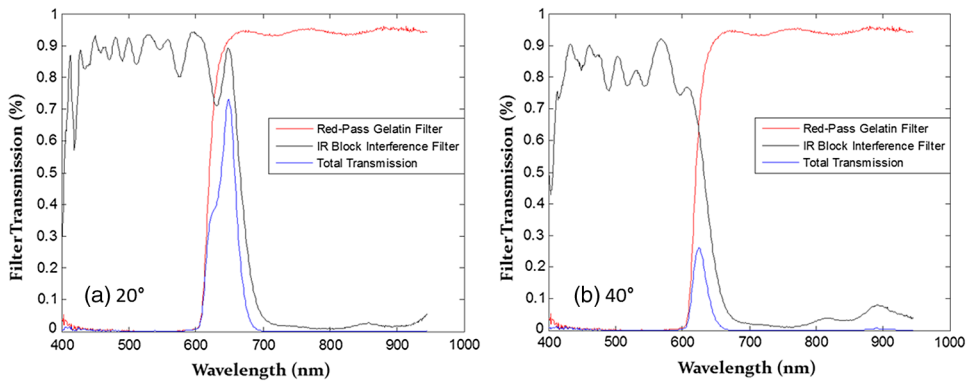

Fig. 5 Red-channel spectral response for each component and for the total filter stack, measured with a fiber-coupled spectrometer: (a) incidence angle = 20 deg; (b) incidence angle = 40 deg. Compare with the on-axis red response in Fig. 4(b).

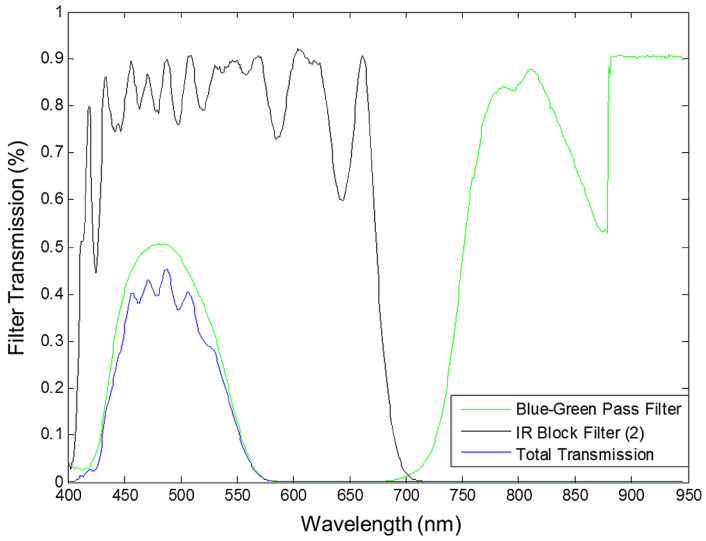

Fig. 6 Spectral transmission function for the blue-green channel in the second-generation imager system. Similar to the red channel, this filter is comprised of stacked IR-block and green-pass filters. The net blue-green response is the lower left curve.

Fig. 7 Photograph of a plywood black-and-white reflectance calibration panel, which is laid on the ground within the imager's field of view to provide a reflectance calibration. Later versions were painted on canvas tarps.

Table 1 lists the primary components used in the second-generation multispectral imaging system, which provided three channels instead of two, in a package that was much lighter than the original system with longer battery life. The table also includes nominal specifications and cost for each component. All components are in the imaging system except the ZigBee coordinator and 5.8-GHz receiver, which are used on the ground with the laptop computer to provide communication with the balloon-borne imager. The table does not include items such as the case, switches, wires, connectors, and so forth. With everything included, the total parts cost for the second-generation, three-channel multispectral imaging system was $1100. The two-channel systems used parts that cost less than $900.

3 Example Data

Ten multispectral imager systems were built and are being used by a wide variety of students for a broad range of applications, but here we show example images obtained during an outreach event with Native American middle-school students at MSU-Bozeman. The imager was attached

Table 1 Parts list for the second-generation multispectral imaging system with nominal specifications and cost.

Component	Specifications	2010 cost	Quantity
M3186A CMOS camera (Electronics123)	200 mW max, 3.7-mm f/2 lens, ~65 × 50 deg FOV, 1/60 to 1/15,000 s integration time, 510 × 492 pixels	$27	3
DVR8106 recording module (Electronics123)	1.8 mW max, 2 GB SD card, 320 × 240 video, 640 × 480 still image capture	$60	3
SD card	2 GB	$6	3
ZR25_ZBMESH ZigBee relay (National Control Devices)	Single-pole double-throw	$93	1
ZBU_COORD ZigBee coordinator (National Control Devices)	5 V USB input	$138	1
NTX100 5.8-GHz video transmitter (Ifrontech)	6 to 15 VDC, ~92 mA	$100	1
NRX Nano 5.8-GHz receiver	6 to 15 VDC, <200 mA	$145	1
Li-ion battery for remote module	10.8 VDC, 2400 mAh	$79	1
NiMH battery for video receiver	12 VDC, 2600 mAh	$30	1
Rosco 38000 IR/UV block filter	1–in. diameter	$6	4
Kodak #29 dark red wratten gel filter	100-mm square sheet→16 filters	$54	1
Kodak #89B NIR pass gel filter	100-mm square sheet→16 filters	$108	1
Kodak #44A blue-green gel filter	75-mm square sheet→16 filters	$95	1

to a helium-filled balloon tethered at an altitude near 50 m on the MSU campus in a region containing a mixture of grass, cement sidewalks, and asphalt streets, as shown in the photograph of Fig. 8. In this photograph, the balloon is near the top, slightly to the right of center, the black-and-white reflectance calibration panel is near the bottom of the picture, just right of center, and the students using a laptop computer with wireless link to control the camera are near the lower left.

Figure 9 shows red and NIR images acquired simultaneously by the balloon-borne imager during this test flight. These images show several features that can be related immediately to the

Fig. 8 Photograph of tethered balloon carrying multispectral imager during test flight at Montana State University. The balloon is located just right of the upper center, and the calibration panel is at the bottom center, next to a parked car.

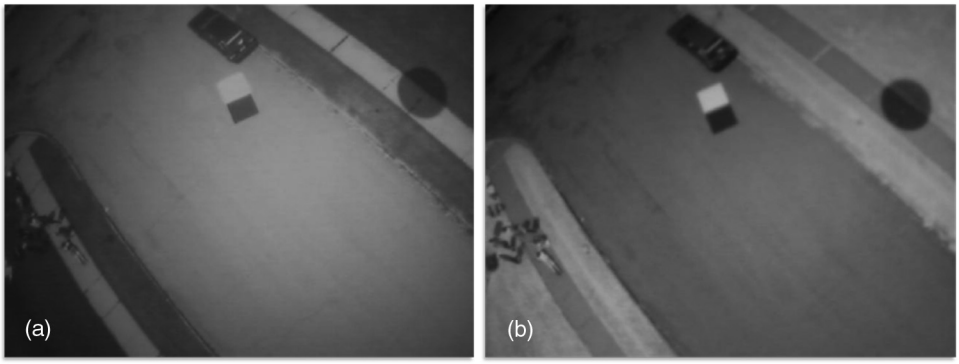

Fig. 9 Images acquired from the balloon-borne multispectral imager: (a) red and (b) NIR.

reflectance spectra of the various regions on the ground. For example, the grass along the lower and upper edges is dark in the red image and very bright in the NIR image, as expected from the reflectance spectra shown in Fig. 1. Also the asphalt street at the center of the image is notably brighter in the red than in the NIR. A similar behavior is observed for the cement sidewalk above and below the asphalt street (with strips of grass on either side). The circular dark region near the upper-right corner of the images is the shadow of the balloon.

Images were retrieved by lowering the balloon, extracting the SD cards, and reading them with the control computer. Once the images were stored on the computer, the image-processing software was used to perform a reflectance calibration. The same image-processing software was also used to align the red-NIR image pairs and to select the pixels containing the black-and-white calibration panel regions. With all of these steps completed, the software was used to calculate the NDVI at each pixel. The resulting NDVI image for this example is shown in Fig. 10, with a color bar that ranges from dark blue denoting NDVI $= -1$ to dark red denoting NDVI $= +1$. This image shows an NDVI pattern that can be explained by the relative dark and bright regions of the images shown in Fig. 9. For example, the grass regions have large, positive NDVI, while the asphalt and concrete regions have large, negative NDVI (indicating that these materials are more highly reflective in the red than in the NIR). Because both the black-and-white regions of the reflectance calibration panel have a relatively flat reflectance spectrum, the NDVI is near zero for both of these regions. The dark strip along the bottom of the NDVI image is where pixels have been ignored after shifting one image with respect to the other to achieve accurate pixel alignment. Imprecise alignment will result in an edge-detection image because of the subtraction in the NDVI calculation.

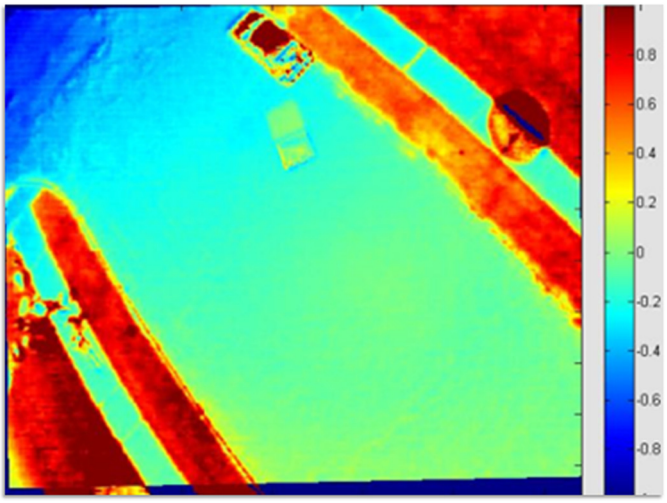

Fig. 10 Normalized difference vegetation index (NDVI) image produced from the red and NIR images in Fig. 8.

4 Conclusion

A low-cost, multispectral imaging system was designed, and 10 copies were built by undergraduate students majoring in electrical engineering, computer engineering, and physics at Montana State University. These imagers, especially the second-generation, three-channel system, provide a useful and effective mechanism to teach principles of optical engineering, imaging, and remote sensing. The imagers operate on a tethered balloon at altitudes up to approximately 50 m. Initial data demonstrate the capability of these low-cost imagers for scene classification using the normalized difference vegetation index to identify vegetation and nonvegetation regions. Future research will explore their use in quantitatively demanding studies that use the NDVI as a measure of plant health.

Acknowledgments

This research was funded by the NASA Minority Serving Institutions Partnership program, through the Montana Space Grant Consortium, via grant NNG05GF08H.

References

1. M. Kamada and T. Okabe, "Vegetation mapping with the aid of low-altitude aerial photography," *Appl. Veg. Sci.* **1**(2), 211–218 (1998), http://dx.doi.org/10.2307/1478950.
2. M. Miyamoto et al., "Use of balloon aerial photography for classification of Kushiro wetland vegetation, northeastern Japan," *Wetlands* **24**(3), 701–710 (2004), http://dx.doi.org/10.1672/0277-5212(2004)024[0701:UOBAPF]2.0.CO;2.
3. H. Suzuki et al., "An ad hoc network in the sky, SKYMESH, for large-scale disaster recovery," in *Proc. IEEE Vehicular Technology Conf.*, pp. 1–5, IEEE, Piscataway, NJ (2006).
4. J. Boike and K. Yoshikawa, "Mapping of periglacial geomorphology using kite/balloon aerial photography," *Permafrost Periglac. Process.* **14**(1), 81–85 (2003), http://dx.doi.org/10.1002/(ISSN)1099-1530.
5. A. T. Mozas-Calvache et al., "Method for photogrammetric surveying of archaeological sites with light aerial platforms," *J. Archaeol. Sci.* **39**(2), 521–530 (2012), http://dx.doi.org/10.1016/j.jas.2011.10.007.
6. V. Tsingas et al., "3D modeling of the Acropolis of Athens using balloon images and terrestrial laser scanning," *Int'l Arch. Photogram. Remote Sens. Spatial Inform. Sci.* **XXXVII** (B5), 1101–1105 (2008).
7. M. O. Altan et al., "Balloon photogrammetry for cultural heritage," *Int'l Arch. Photogram. Remote Sens. Spatial Inform. Sci.* **XXXVII**(B5), 964–968 (2004).
8. J. A. J. Berni et al., "Thermal and narrowband multispectral remote sensing for vegetation monitoring from an unmanned aerial vehicle," *IEEE Trans. Geosci Remote Sens.* **47**(3), 722–738 (2009), http://dx.doi.org/10.1109/TGRS.2008.2010457.
9. S. R. Herwitz et al., "Imaging from an unmanned aerial vehicle: agricultural surveillance and decision support," *Comput. Electron. Agr.* **44**(1), 49–61 (2004), http://dx.doi.org/10.1016/j.compag.2004.02.006.
10. N. E. Hulst et al., "AgCam: scientific imaging from the ISS window observational research facility," in *Proc. IEEE Aerospace Conf.*, pp. 11–21, IEEE, Piscataway, NJ (2004).
11. D. Olsen et al., "Radiometric calibration for AgCam," *Remote Sens.* **2**(2), 464–477 (2010), http://dx.doi.org/10.3390/rs2020464.
12. J. H. Rouse et al., "Multi-spectral imaging of vegetation for detecting CO_2 leaking from underground," *Environ. Earth Sci.* **60**(2), 313–323 (2010), http://dx.doi.org/10.1007/s12665-010-0483-9.
13. A. Hogan et al., "Low-cost multispectral vegetation imaging system for detecting leaking CO_2 gas," *Appl. Opt.* **51**(4), 59–66 (2012), http://dx.doi.org/10.1364/AO.51.000A59.
14. J. A. Hogan et al., "Detection of leaking CO_2 gas with vegetation reflectance measured by a low-cost multispectral imager," *IEEE J. Sel. Top. Appl. Earth Obs. Remote Sens.* **5**(3), 699–706 (2012), http://dx.doi.org/10.1109/JSTARS.2012.2202880.
15. C. J. Keith et al., "Monitoring effects of a controlled subsurface carbon dioxide release on vegetation using a hyperspectral imager," *Int. J. Greenhouse Gas Control* **3**(5), 626–632 (2009), http://dx.doi.org/10.1016/j.ijggc.2009.03.003.

16. E. J. Male et al., "Using hyperspectral plant signatures for CO_2 leak detection during the 2008 ZERT CO_2 sequestration field experiment in Bozeman, Montana," *Environ. Earth Sci.* **60**(2), 251–261 (2010), http://dx.doi.org/10.1007/s12665-009-0372-2.
17. L. H. Spangler et al., "A shallow subsurface controlled release facility in Bozeman, Montana, USA, for testing near surface CO_2 detection techniques and transport models," *Environ. Earth Sci.* **60**(2), 227–239 (2010), http://dx.doi.org/10.1007/s12665-009-0400-2.
18. J. R. Jensen, *Remote Sensing of the Environment: An Earth Resource Perspective*, Prentice-Hall Publishers, Upper Saddle River, NJ (2000).
19. J. M. Eichenholz and J. Dougherty, "Ultracompact fully integrated megapixel multispectral imager," *Proc. SPIE* **7218**, 721814 (2009), http://dx.doi.org/10.1117/12.809527.
20. S. A. Mathews, "Design and fabrication of a low-cost, multispectral imaging system," *Appl. Opt.* **47**(28), F71–F76 (2008), http://dx.doi.org/10.1364/AO.47.000F71.
21. J. S. Tyo et al., "Review of passive imaging polarimetry for remote sensing applications," *Appl. Opt.* **45**(22), 5453–5469 (2006), http://dx.doi.org/10.1364/AO.45.005453.
22. E. L. Dereniak and G. D. Boreman, *Infrared Detectors and Systems*, John Wiley & Sons Publishers, New York, NY (1996).

Joseph A. Shaw is the director of the Optical Technology Center, professor of electrical and computer engineering, and affiliate professor of physics at Montana State University in Bozeman, Montana. He received PhD and MS degrees in optical sciences from the University of Arizona, an MS degree in electrical engineering from the University of Utah, and a BS degree in electrical engineering from the University of Alaska–Fairbanks. He conducts research on the development and application of radiometric, polarimetric, and laser-based optical remote sensing systems. He is a fellow of the OSA and SPIE.

Paul W. Nugent is a research engineer with the Electrical and Computer Engineering Department at Montana State University and president of NWB Sensors Inc., in Bozeman, Montana. He received his MS and BS degrees in electrical engineering from Montana State University. His research activities include radiometric thermal imaging and optical remote sensing.

Nathan A. Kaufman graduated from Montana State University in Bozeman, Montana, with a BS degree in electrical engineering. During his undergraduate phase, he performed remote-sensing based research in the optical remote sensor lab headed by Dr. Joseph Shaw. His main topics of focus were LIDAR data analysis, remote climate sensor data transfer, and the development of low-cost multispectral imagers. He currently works in Bozeman as an electrical design engineer at Quantum Composers, he performs custom electronics and instrumentation design for pulse generators, custom controls, and laser systems.

Nathan J. Pust is a research engineer working at Montana State University. He received bachelor degrees in electrical engineering and computer engineering from Montana State University in 2002 and his PhD in electrical engineering from Montana State University in 2007.

Randal M. Larimer received his MSEE in 1982 from Montana State University–Bozeman, his BSEE in 1980 from the University of Illinois Urbana–Champaign, and his AS in physics in 1978 from Black-Hawk College–Moline, Illinois. He has 30 years of electrical engineering experience in a variety of positions and product areas. Currently he is the deputy director of the Montana Space Grant Consortium (NASA) working on the Minority Serving Institute Tribal College Partnership Development Program, the IRIS National Student Solar Spectrograph Competition, the BOREALIS high altitude ballooning program, and activities supporting the director and the Space Grant Program locally, statewide, and nationally. He also teaches classes as an adjunct assistant professor in the Electrical and Computer Engineering Department at Montana State University. He is a senior member of the IEEE.

Angela C. DesJardins is the director of the Montana Space Grant Consortium (MSGC) and Montana NASA EPSCoR (MNE). MSGC and MNE are NASA programs that work to strengthen research and education in Montana in aerospace science and engineering fields. She is highly involved in the national leadership of Space Grant, serving on both the National Space Grant Alliance and National Space Grant Foundation boards. Within Montana, she also serves several education and research communities via advisory board positions and service activities. A solar physicist by training, she continues to stay connected to research and advises solar research students in the summer. Her goal is to encourage Montana students to get involved in space activities.

W. Berk Knighton received his BS (chemistry) in 1978, MS (physical chemistry) in 1980, and PhD (analytical chemistry) in 1984 from Montana State University. He was an assistant professor of chemistry at Franklin and Marshall College from 1984 to 1987 before returning to Montana State University as research associate. He is currently a research professor in chemistry and the flight director of Montana State University's high altitude ballooning program. As flight director, he supervises undergraduate students in the development of balloon-borne research projects.

Biographies and photographs of the other authors are not available.